Eur. Phys. J. C (2018) 78:973
https://doi.org/10.1140/epjc/s10052-018-6462-0

THE EUROPEAN PHYSICAL JOURNAL C

Regular Article - Experimental Physics

The $Na_2W_2O_7$ crystal: a crystal scintillator for dark matter search experiment

Indra Raj Pandey[1], H. J. Kim[1,a], H. S. Lee[2], Y. D. Kim[2], M. H. Lee[2], V. D. Grigorieva[3], V. N. Shlegel[3]

[1] Department of Physics, Kyungpook National University, Daegu 41566, South Korea
[2] Center for Underground Physics, Institute for Basic Science (IBS), Daejeon 34126, South Korea
[3] Nikolaev Institute of Inorganic Chemistry, SBRAS, Novosibirsk 630090, Russia

Received: 21 February 2018 / Accepted: 16 November 2018 / Published online: 24 November 2018

Abstract A single crystal of $Na_2W_2O_7$ (NWO) was grown by a low-thermal-gradient Czochralski technique (LTG-CZ). The scintillation properties of the crystal were evaluated for the first time as a potential material for dark matter search experiments. The luminescence and scintillation characteristics of the crystal were studied at room temperature and low temperatures by using a light-emitting diode (LED) and a ^{90}Sr beta source. The luminescence and scintillation light yield at 10 K were significantly higher than those at room temperature. The crystal showed higher light yield at 10 K than a $CaMoO_4$ (CMO) crystal. The decay time of the crystal was investigated at temperatures between 10 and 300 K. The sensitivity to spin-independent weakly interacting massive particle-nucleon interactions based on 10 kg (2 months) and 50 kg (12 months) data for the NWO crystal detectors was estimated by a simulated experiment using the standard halo model. The luminescence, scintillation, and sensitivity results revealed that the NWO crystal is a promising candidate for a dark matter search experiment in the near future.

1 Introduction

It is now generally accepted in the scientific community that the majority of the matter in our universe is invisible, exotic, and nonbaryonic dark matter [1–3]. Weakly Interacting Massive Particles (WIMPs) are one of the stringent candidates for the dark matter well motivated by cosmology and supersymmetric models [4–6]. The WIMPs can be detected directly [7,8] by measuring the recoil energy from a target nucleus when the WIMPs collide with the nucleus in a target materials. Among various experimental results on the WIMPs search; only DAMA and DAMA/LIBRA are continuously reporting a significant annual modulation signal by using a NaI(Tl) scintillating crystal [9]. But, the modulation signal given by the DAMA/LIBRA has been a subject of continuing debate because other experiments such as XMASS, Super-CDMS, LUX, PandaX, XENON, KIMS, CRESST observed null signals in the regions of the WIMP-nucleon cross-section and WIMP-mass parameter space favored by the DAMA/LIBRA observations [10–16]. However, it is possible to explain all of the direct search experiments' results in terms of non-trivial systematic differences in detector responses and possible modifications of the commonly used halo model on the galactic distribution of dark matter [17,18]. At the same time, to resolve the puzzling status between the DAMA and other experiments, it is necessary to use the same target materials with higher sensitivity for the WIMP interaction. WIMP-Iodine interpretation of the DAMA signal was ruled out by the same iodine target from the KIMS experiment [15]. However, low mass WIMP-Sodium interaction is not covered by the same sodium target yet.

To achieve high sensitivity to rare events, detection techniques discriminating extremely rare signals from significant radioactive backgrounds are necessary. One of the most promising techniques is a cryogenic phonon scintillation detector (CPSD) technique, which can discriminate γ/e^- backgrounds from nuclear recoil signals [19–21]. $CaWO_4$ was the first crystal used in a cryogenic dark matter search experiment (CRESST) owing to its high light yield at low temperature [22]. The Advanced Mo-based Rare process Experiment (AMoRE) project has a series of experiments using a CMO scintillating crystal and advanced cryogenic techniques to search for rare events such as; neutrinoless double-beta decay and dark matter [23]. The main background source in the CMO crystal is ^{226}Ra (from ^{238}U family), and purification of a Ca-based compound below acceptable radioactivity level is a significant challenge due to constraints imposed by some calcium chemistry [24]. In this work, we discuss the luminescence and the scintillation prop-

[a] e-mail: hongjoo@knu.ac.kr

erties and expected sensitivity of the NWO crystal. The advantages of this scintillator are; large crystals can be grown, the material works successfully at cryogenic temperatures, the light yield at low temperature (10 K) is higher than that of CMO crystal although it is very low at room temperature, and purification techniques for Na and W are already well developed [9,25,26]. Furthermore, the same sodium target with the DAMA-NaI experiment will bring less model dependent conclusion on the interpretation of WIMP-Sodium interaction of the DAMA signals. In a future prospect, this crystal with the CPSD technique has a potential for the WIMP search by validating the annual modulation claim by the DAMA/LIBRA [9].

2 Material and methods

2.1 Crystal growth

High-quality powders of Na_2CO_3 and WO_3 were used as starting materials for growing the crystals. The crystal was grown at Nikolaev Institute of Inorganic Chemistry, Siberian Branch, Russian Academy of Science, at Novosibirsk, Russia, using the LTG-CZ technique. A large single crystal of dimensions $\sim$35 mm (diameter) $\times$ 60 mm (length) along the [001] direction was produced by this technique; the crystal growth process is described in Ref. [27]. The crystal structure is orthorhombic with space group Cmca and consists of chains of WO_6^{6-} octahedra and WO_4^{2-} tetrahedra [28]. Figure 1 shows photographs of the grown crystal and the samples of NWO and CMO measured in this work.

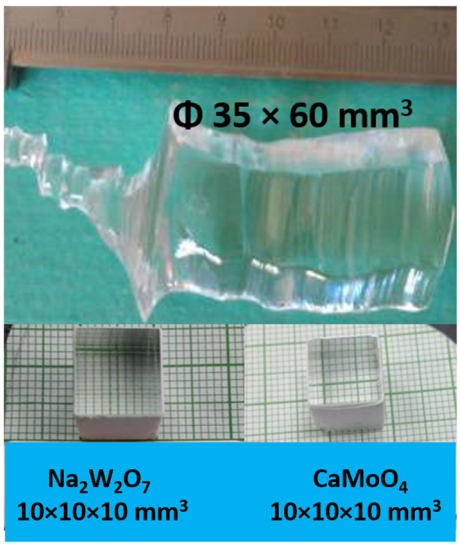

Fig. 1 Photographic views of grown NWO crystal and measured samples of NWO and CMO crystals

2.2 Instrumentation for test setup

Transmittance spectra were recorded by using a V-650 spectrophotometer (Jasco). Figure 2 shows a schematic diagram of the experimental setup for characterization of the crystals. A $10 \times 10 \times 10$ mm^3 sample was placed inside the cryostat. There was one optical window outside the cryostat chamber to allow a light from a light-emitting diode (LED) to stimulate the crystal. The light from the LED was guided by a hollow Teflon tube. The crystal was excited by a 280-nm-wavelength LED source, and the power for the LED was supplied by a function generator. A thermal grease (Apiezon Products, M&I Materials Ltd.) was used to couple the crystal to a cold finger. Three sides of the crystal were wrapped with a 250-μm-thick Teflon sheet as a light reflector. The luminescence light from the crystal sample was sent to a photomultiplier tube (PMT, XP2260, Photonis) or a convex lens waveguide through a quartz light guide for decay time or luminescence spectrum measurement, respectively. The signal from the PMT was sent to a 600-MHz-bandwidth oscilloscope (LeCroy WaveRunner 64Xi-A) for decay time analysis, whereas the signal from waveguide was sent to a spectrometer (QE65000, Ocean Optics) and a computer for emission spectrum analysis.

The scintillation properties of the crystals were measured by a single-photon-counting technique using a ^{90}Sr beta source as the excitation source. Two layers of 250-μm-thick Teflon sheets were used as the light reflector on four sides of the crystal (except the top and bottom). The source was fully attached to one side of the crystal by the Teflon sheet. An R7400U-20 (Hamamatsu multi-alkali) PMT was optically coupled to a quartz light guide using optical grease (EJ-550 Optical Grade Silicone Grease). The signal from the PMT was sent to a preamplifier having a gain of 50 times and then to a flash analog-to-digital converter (NOTICE KOREA) [29].

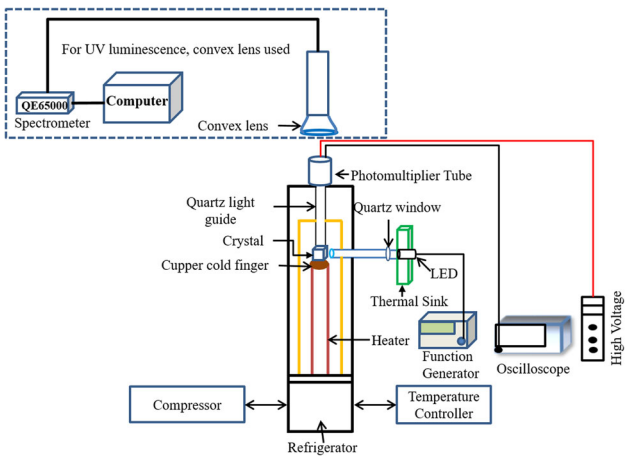

Fig. 2 A Schematic diagram of the low temperature setup for luminescence decay time and light yield measurement

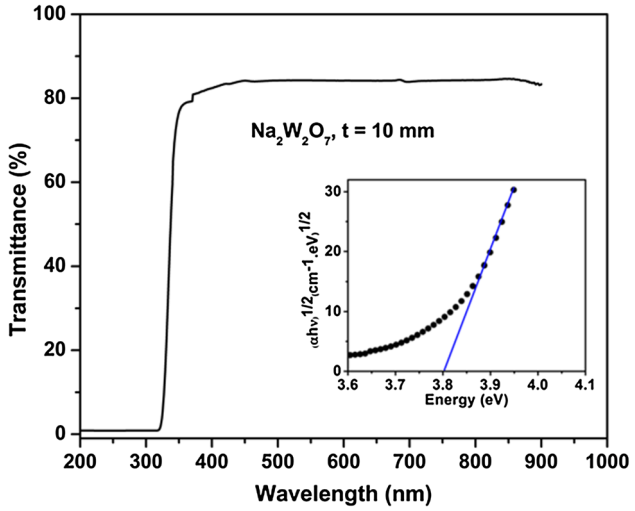

Fig. 3 Transmittance spectrum of a NWO crystal with thickness of 10 mm. Inset figure shows the energy band gap calculation of the crystal

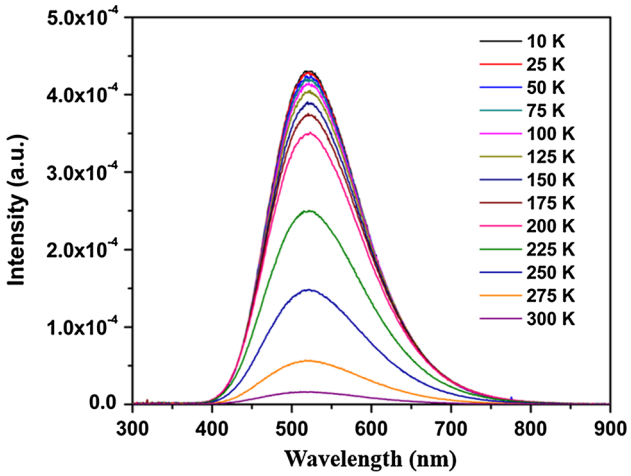

Fig. 4 Luminescence spectra of a NWO crystal at different temperatures

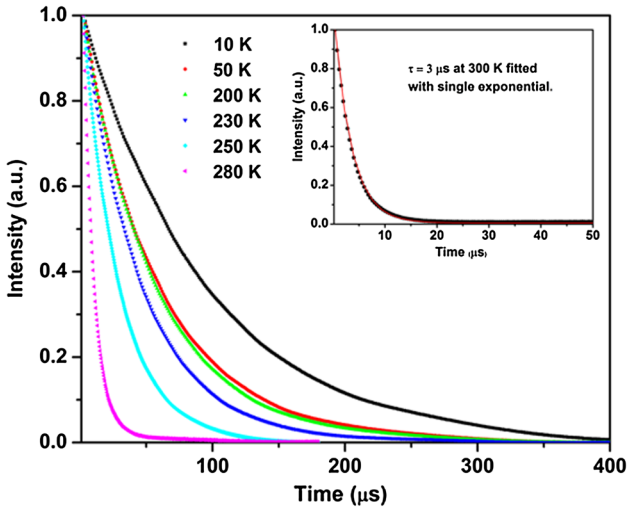

Fig. 5 Luminescence decay curves of a NWO crystal at different temperatures; inset shows a single exponential fit to the data at room temperature

2.3 Ultraviolet-visible to near-infrared spectral analysis

Figure 3 shows the transmittance spectrum of the grown crystal at room temperature. The total transmittance is almost flat (∼84%) in the visible to near-infrared region (320–900) nm considering without surface reflection. Because of the fundamental absorption characteristics of the NWO crystal, it has a wavelength cutoff in the 320 nm region. A relation between the optical absorption coefficient (α) and the optical band gap is expressed to calculate the energy band gap of the crystal by using the following relation [30],

$$\alpha(\nu) = A\frac{(h\nu - E_g)^n}{h\nu} \quad (1)$$

where, $n = 2$ for indirect transition, A is a normalization constant, h is Panck's constant and ν is frequency. By using the above equation, and plotting $(\alpha h\nu)^{1/2}$ Vs photon energy ($h\nu$), the optical energy band gap (E_g) for indirect transition was calculated by extrapolating the linear region of the curve to the x-axis as shown in the inset of Fig. 3. The indirect energy gap is found to be ∼3.80 eV.

2.4 Luminescence properties

The temperature-dependent luminescence light yield and decay time are studied to investigate the scintillation process in the material. NWO crystals as a detector material must exhibit several low-temperature characteristics. Among them, the luminescence properties are the most important [31]. Using an LED excitation source, the temperature dependent luminescence properties of the crystal are studied at temperatures from 300 to 10 K, and the results are shown in Fig. 4. At room temperature, weak luminescence is observed between 340 and 790 nm, with a peak at 515 nm. When the crystal is cooled to 10 K, the emission intensity increases by ∼20 times, in the range of 320 to 915 nm and a peak appears at 520 nm. The luminescence emission of the NWO crystal at 520 nm is attributed to the WO_6^{6-} octahedral group [28].

The luminescence decay times at different temperatures are shown in Fig. 5. At high temperatures, the decay constant is well fitted with a single exponential; however, at low temperatures (< 50 K), it is fitted with two exponentials. The inset of Fig. 5 shows a decay curve at room temperature fitted by a single exponential. A fast decay time constant of ∼3 μs is observed at room temperature, and the decay constant is 94 μs at 10 K. Figure 6 shows the temperature dependence decay time from room temperatures (300 K) to 10 K. The decay time steeply rises in between 300 and 200 K. From

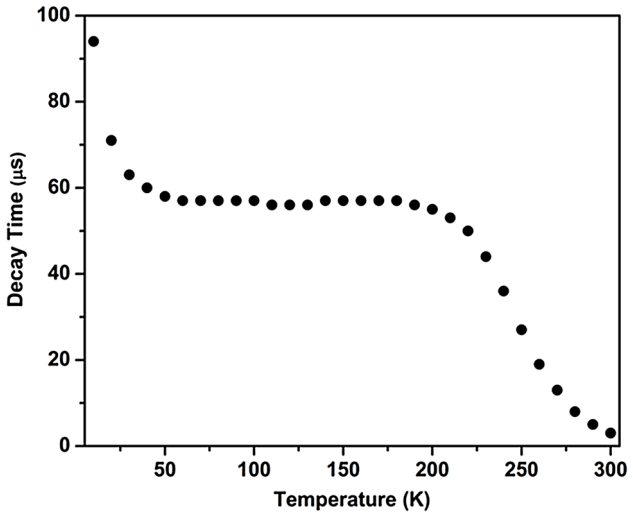

Fig. 6 Decay constants of a NWO crystal as a function of temperature

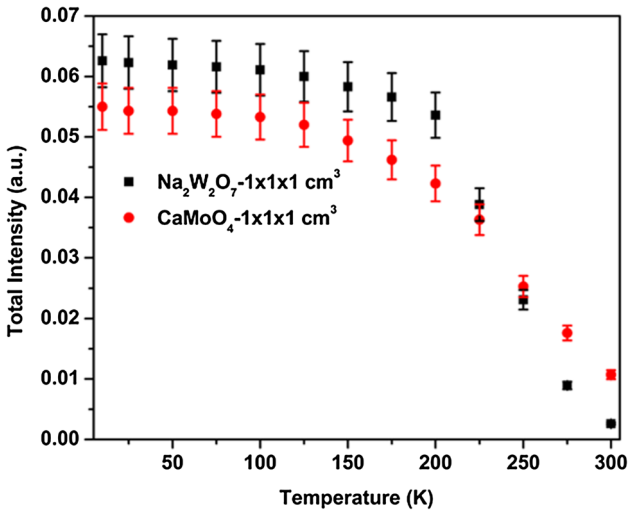

Fig. 7 Luminescence light yields comparison of NWO and CMO crystal at different temperatures, using a 280-nm-wavelength LED excitation source

200 to 30 K, however, the decay profile is constant. Another rise in the decay time constant is observed as the temperature decreases from 30 to 10 K. Overall, the observed decay time constant increases by a factor of ∼31 from 300 to 10 K.

The total intensities of NWO and CMO crystals were measured under the same conditions at different temperatures, which is shown in Fig. 7. The reference CMO crystal was supplied by the Institute for Materials (Lviv, Ukraine); it is denoted as CMO-4 and has the highest light yield among the CMO crystals reported in Ref. [32]. In Fig. 7, a total systematic error of 7% was added to account for the angle and position dependence of the crystal. The temperature dependence of the luminescence light yield of the CMO crystal is similar to the result reported in Ref. [33]. As shown in Fig. 7, the luminescence light yield of NWO crystal was lower than that of CMO at above ∼250 K. However, as the temperature decreased further to 10 K, the light yield of NWO increased significantly and exceeded that of CMO. The low light yield at high temperature might be due to a thermal quenching effect, in which the emission intensity decreases because of the higher probability of nonradiative transitions at high temperature [34]. The luminescence light yield of the NWO crystal increased by a factor of 24 as the temperature decreased from 300 to 10 K and was 114% of that of the CMO crystal at 10 K.

2.5 Scintillation properties

The scintillation properties of the crystal were studied by a single-photon-counting technique based on the recording of individual photons from scintillation events. This is especially useful for slow scintillation process elements to avoid pileup problems. Figure 8 compares the temperature-dependent scintillation light yields of the NWO and CMO crystals. The scintillation light yield pattern of the CMO crystal matches the result in Ref. [35] well. At high temperature (250–300 K), the light yield of the NWO crystal is lower than that of CMO; at room temperature, it is 26% of that of the CMO crystal. The low light yield at high temperature might be due to a thermal quenching effect. Below 250 K, the light yield increases significantly and becomes higher than that of the CMO crystal. The maximum light yield is achieved at 150 K, but further cooling to 50 K decreases the light yield. The decrease in the light yield in this temperature region might be due to traps in the crystal because of impurities or crystal defects. Under further cooling from 50 to 10 K, the light yield increases again, and at 10 K it is 13 times that at 300 K. At 10 K, the scintillation light

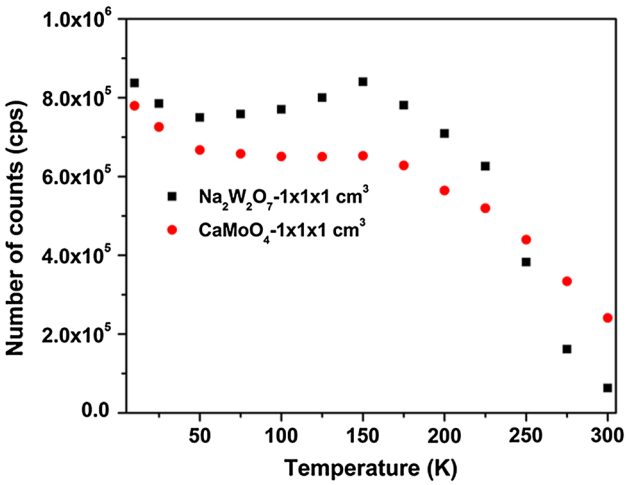

Fig. 8 Temperature dependent scintillation light yield comparison of NWO and CMO crystals using ^{90}Sr beta source as the excitation source

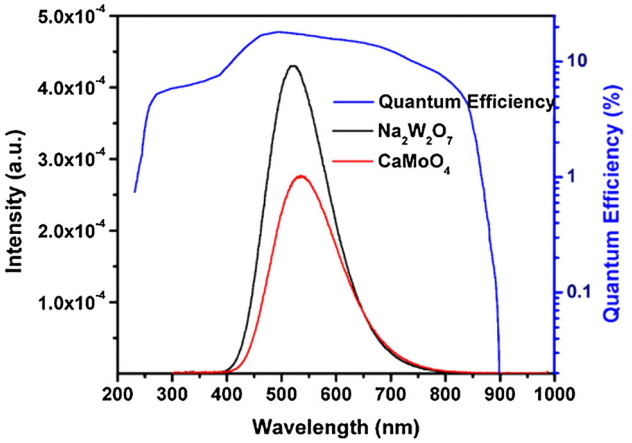

Fig. 9 Emission spectra of NWO and CMO at 10 K along with QE spectrum of the PMT

yield of the NWO crystal is 107% of that of the CMO crystal. It can be easily increased in the future by improving the crystal quality and optimizing the post growth heat treatment. Owing to improvements in the quality of crystals grown by various companies, the light yield of CMO crystals increased by ∼20% [32]. In addition, annealing can modify the defects in the crystals and change their scintillation and luminescence properties noticeably. After annealing treatments under different environmental conditions, the light yields of the tungstate crystals $PbWO_4$ [36], $ZnWO_4$ [37], and $CaWO_4$ [38,39] increased significantly (up to 50% for $CaWO_4$).

Figure 9 shows the emission spectra of the CMO and NWO crystals at 10 K and the quantum efficiency (QE) spectrum of the R7400U-20 (Hamamatsu) PMT. The emission peaks of the NWO and CMO crystals appear at 520 and 540 nm, respectively. Because the emission peaks of the measured samples are not in the same range, the emission-weighted quantum efficiency ($\overline{EMQE}$) values of the PMT for NWO and CMO were calculated from the emission spectra of the crystals at 10 K and the QE spectrum of PMT according to the following equation (2) [40].

$$\overline{EMQE} = \frac{\int QE(\lambda)Em(\lambda)d(\lambda)}{\int Em(\lambda)d(\lambda)} \quad (2)$$

where, QE(λ) and Em(λ) are the QE and emission probability of the crystal, respectively, as a function of wavelength. The $\overline{EMQE}$ values of the PMT for NWO and CMO were found to be 16.45% and 16.22%, respectively.

3 Predicted sensitivity of $Na_2W_2O_7$ crystal

To test the feasibility of NWO crystals for low mass WIMP search, we estimate the sensitivity of the WIMP-nucleon spin-independent interaction, with assumptions on detector performance, background reduction, and exposure. The calculated limits are compared with recent results from direct detection experiments. We model the signal on the spin-independent WIMP-nucleon interaction in NWO crystal detectors as a function of recoil energy, which was estimated in the context of the standard halo model [41]. Specifically, a Maxwellian velocity distribution was assumed for dark matter with the WIMP characteristic velocity v_0 of 230 km/s, mean earth velocity V_E of 232 km/s, local galactic escape velocity V_{esc} of 544 km/s, and dark matter density ρ_D of 0.3 GeV/cm^3 [42–44].

Since we have not developed low temperature detector with NWO crystals yet, experimental parameters are unavailable. We therefore make assumptions on detector performance based on the recent development of a similar type of detector with CaWO4 crystal for the CRESST experiment [16,45–47]. A low energy threshold of 0.3 keV with a 300 g detector module has been achieved with 0.09 ± 0.01 keV energy resolution at 2.6 keV [16,45]. Considering the sufficiently high light yield of the crystal at low temperature, we assume a similar level of β and γ leakage into the acceptance region from Ref. [45–47], which are nearly 10% at (0.5–1) keV, 1% at (1–3) keV, and 0.1% above 3 keV. Energy resolution is assumed to be 0.1 keV in the low energy region. We consider a two step experimental approach with proper developments of low-temperature detector [48] and active background reduction of the detectors, which are actively ongoing in South Korea [49,50]. At first phase, we consider 10 kg detectors corresponding to 20–30 detector modules with 1 counts/keV/kg/day background, 600 kg days exposure time, and 1 keV energy threshold. Further development for next phase can be realized with 50 kg detectors corresponding to 100–150 detector modules with 0.1 counts/keV/kg/day background, 18,250 kg days exposure, and 0.5 keV energy threshold. Table 1 shows a summary of assumed parameter for two different phases of experiments along with the parameters measured by the CRESST experiment. In both cases, a flat background and a step-like energy threshold is assumed. The result of the calculated sensitivity on the WIMP-nucleon spin-independent cross section is shown in Fig. 10, which is compared with the results of CRESST 2016 [51], LUX 2017 [52], XENON1T 2017 [14], and CDMSlite 2016 [53].

4 Conclusion

The scintillation as well as luminescence properties of a NWO crystal were studied at room and cryogenic temperatures by using an LED and a ^{90}Sr beta source. The emission spectrum of the sample under an LED (280 nm) irradiation at 10 K showed the maximum intensity. The luminescence decay time was 3 μs at 300 K and 94 μs at 10 K, which is

Table 1 Summary table of assumed parameters for two different phase of experiment, which is compared with CRESST parameter

Experiment	Crystal	Crystal mass (g)	Total mass (kg)	Exposure time (kg days)	Energy threshold (keV)	Background (counts/keV/kg/day)
Phase-1	$Na_2W_2O_7$	300	10	600	1	1
Phase-2	$Na_2W_2O_7$	300	50	18250	0.5	0.1
CRESST-II Phase 2	$CaWO_4$	300	5	29	0.3	3.51 [16,45]
CRESST-III Phase 1	$CaWO_4$	24	0.25	50	0.1	3.44 [47,51]

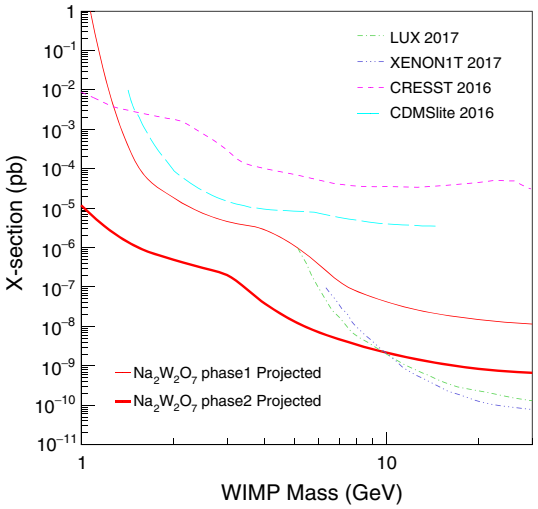

Fig. 10 Expected 90% confidence level limits on the WIMP-nucleon spin-independent (SI) cross section with NWO crystals are presented. Thin red solid line represents a case of 10 kg NWO crystal, 1 counts/keV/kg/day background, and 1 keV energy threshold and thick red solid line corresponds to a case of 50 kg crystal, 0.1 counts/keV/kg/day background, and 0.5 keV energy threshold

about 31 times. At 10 K, the luminescence and scintillation light yield of the crystal was 114% and 107% respectively as compared to that of a CMO crystal. The light yield of the crystal can be increased easily in future by improving the crystal quality and optimizing the annealing conditions. The projected sensitivity plots obtained for 10 and 50 kg of NWO crystals show significant results at low energy (10 to 1 GeV) compared to those of other experimental groups results. Because of the high light yield at low temperature and a good sensitivity to the low-mass WIMP signal; this crystal will be a promising scintillator for dark matter searches at cryogenic temperatures.

Acknowledgements This investigation was supported by the National Research Foundation of Korea (NRF) funded by the Korean government (MEST) (Nos. 2018R1A2A1A05022079 and 2018R1A6A1A06024970).

References

1. P.A.R. Ade, Planck Collaboration, A&A **594**, A3 (2016). https://doi.org/10.1051/0004-6361/201526998
2. J.L. Feng, Annu. Rev. Astron. Astrophys. **48**, 495 (2010). https://doi.org/10.1146/annurev-astro-082708-101659
3. N.A. Bahcall, Science **284**, 1481 (1999). https://doi.org/10.1126/science.284.5419.1481
4. B.W. Lee, S. Weinberg, Phys. Rev. Lett. **39**, 165 (1977). https://doi.org/10.1103/PhysRevLett.39.165
5. G. Jungman et al., Phys. Rep. **267**, 195 (1996). https://doi.org/10.1016/0370-1573(95)00058-5
6. G. Bertone, Nature **468**, 389 (2010). https://doi.org/10.1038/nature09509
7. R.J. Gaitskell, Annu. Rev. Nucl. Part. Sci. **54**, 315 (2004). https://doi.org/10.1146/annurev.nucl.54.070103.181244
8. M. Pospelov et al., Phys. Rev. D **89**, 055008 (2014). https://doi.org/10.1103/PhysRevD.89.055008
9. R. Bernabei et al., Eur. Phys. J. C **73**, 2648 (2013). https://doi.org/10.1140/epjc/s10052-013-2648-7
10. K. Abe, XMASS Collaboration, Phys. Lett. B **759**, 272 (2016). https://doi.org/10.1016/j.physletb.2016.05.081
11. R. Agnese, SuperCDMS Collaboration, Phys. Rev. Lett. **112**, 241302 (2014). https://doi.org/10.1103/PhysRevLett.112.241302
12. D.S. Akerib, LUX Collaboration, Phys. Rev. Lett. **118**, 021303 (2017). https://doi.org/10.1103/PhysRevLett.118.021303
13. A. Tan, PandaX Collaboration, Phys. Rev. Lett. **117**, 121303 (2016). https://doi.org/10.1103/PhysRevLett.117.121303
14. E. Aprile, XENON Collaboration, Phys. Rev. Lett. **121**, 111302 (2018). https://doi.org/10.1103/PhysRevLett.121.111302
15. S.C. Kim, KIMS Collaboration, Phys. Rev. Lett. **108**, 181301 (2012). https://doi.org/10.1103/PhysRevLett.108.181301
16. G. Angloher, CRESST Collaboration, Eur. Phys. J. C **76**, 25 (2016). https://doi.org/10.1140/epjc/s10052-016-3877-3
17. C. Arina et al., Phys. Rev. Lett. **114**, 011301 (2015). https://doi.org/10.1103/PhysRevLett.114.011301
18. R. Bernabei, EPJ Web Conf. **70**, 00043 (2014). https://doi.org/10.1051/epjconf/20147000043
19. V.B. Mikhailik, H. Kraus, J. Phys. D Appl. Phys. **39**, 1181 (2006). https://doi.org/10.1088/0022-3727/39/6/026
20. J.H. Lee, Nucl. Instrum. Methods A **782**, 133 (2015). https://doi.org/10.1016/j.nima.2015.02.011
21. J.B. Birks, *The Theory and Practice of Scintillation Counting* (Pergamon Press, Oxford, 1964)
22. R.F. Lang, W. Seidel, New J. Phys. **11**, 105017 (2009). https://doi.org/10.1088/1367-2630/11/10/105017
23. V. Alenkov et al. (2015). arXiv:1512.05957v1

24. V.B. Mikhailik, H. Kraus, Phys. Status Solidi B **247**, 1583 (2010). https://doi.org/10.1002/pssb.200945500
25. G. Adhikari et al., Eur. Phys. J. C **77**, 437 (2017). https://doi.org/10.1140/epjc/s10052-017-5011-6
26. A. Munster et al., J. Cosmol. Astropart. P **05**, 018 (2014). https://doi.org/10.1088/1475-7516/2014/05/018
27. T.A. Gavrilova et al., Solid State Phenom. **213**, 160 (2014). https://doi.org/10.4028/www.scientific.net/SSP.213.160
28. W. Qin-Hua et al., Chin. Phys. Lett. **28**, 118104 (2011). https://doi.org/10.1088/0256-307x/28/11/118104
29. http://www.noticekorea.com/
30. E.M. Yoshimura et al., Opt. Mater. **31**, 795 (2009). https://doi.org/10.1016/j.optmat.2008.08.004
31. M.X. Xue, Chin. Phys. C **41**, 046002 (2017). https://doi.org/10.1088/1674-1137/41/4/046002
32. A.N. Annenkov, Nucl. Instrum. Methods A **584**, 334 (2008). https://doi.org/10.1016/j.nima.2007.10.038
33. D.A. Spassky et al., Opt. Mater. **35**, 2465 (2013). https://doi.org/10.1016/j.optmat.2013.06.054
34. V.B. Mikhailik et al., Phys. Rev. B **75**, 184308 (2007). https://doi.org/10.1103/PhysRevB.75.184308
35. V.B. Mikhailik, Nucl. Instrum. Methods A **583**, 350 (2007). https://doi.org/10.1016/j.nima.2007.09.020
36. W. Zhu, Phys. B **324**, 53 (2002). https://doi.org/10.1016/S0921-4526(02)01269-3
37. I. Bavykina et al., Opt. Mater. **31**, 1382 (2009). https://doi.org/10.1016/j.optmat.2008.09.018
38. V. Yakovyna et al., Opt. Mater. **30**, 1630 (2008). https://doi.org/10.1016/j.optmat.2007.11.003
39. Mv Sivers et al., Opt. Mater **34**, 1843 (2012). https://doi.org/10.1016/j.optmat.2012.05.014
40. C. Leroy, P.G. Rancoita, *Principles of Radiation Interaction in Matter and Detection*, 4th edn. (World Science, Singapore, 2016). https://doi.org/10.1142/9167
41. A.K. Drukier et al., Phys. Rev. D **33**, 3495 (1986). https://doi.org/10.1103/PhysRevD.33.3495
42. J.D. Lewin, P.F. Smith, Astropart. Phys. **6**, 87 (1996). https://doi.org/10.1016/S0927-6505(96)00047-3
43. D.S. Akerib, CDMS Collaboration, Phys. Rev. D **68**, 082002 (2003). https://doi.org/10.1103/PhysRevD.68.082002
44. A.J.K. Chua et al., Eur. Phys. J. C **73**, 2259 (2013). https://doi.org/10.1140/epjc/s10052-012-2259-8
45. R. Strauss, CRESST Collaboration, Eur. Phys. J. C **75**, 352 (2015). https://doi.org/10.1140/epjc/s10052-015-3572-9
46. F. Petricca et al., CRESST Collaboration (2017). arXiv:1711.07692
47. R. Strauss, CRESST Collaboration, J. Phys. Conf. Ser. **718**, 042048 (2016). https://doi.org/10.1088/1742-6596/718/4/042048
48. H.S. Jo, AMoRE Collaboration, J. Phys. Conf. Ser. **888**, 012232 (2017). https://doi.org/10.1088/1742-6596/888/1/012232
49. K.A. Shin et al., J. Radioanal. Nucl. Chem. **317**, 1329 (2018). https://doi.org/10.1007/s10967-018-6006-y
50. O. Gileva et al., J. Radioanal. Nucl. Chem. **314**, 1695 (2017). https://doi.org/10.1007/s10967-017-5568-4
51. M. Willers, CRESST Collaboration, J. Phys.: Conf. Ser. **888**, 012209 (2017). https://doi.org/10.1088/1742-6596/888/1/012209
52. D.S. Akerib, LUX Collaboration, Phys. Rev. Lett. **118**, 251302 (2017). https://doi.org/10.1103/PhysRevLett.118.251302
53. R. Agnese, SuperCDMS Collaboration, Phys. Rev. Lett. **116**, 071301 (2016). https://doi.org/10.1103/PhysRevLett.116.071301